Landau Levels and Electronic States for Pseudospin-1 Lattices with a Bandgap: Application to a Lieb Lattice

Liubov Zhemchuzhna *, Lovely Joseph, Andrii Iurov *, Godfrey Gumbs, Danhong Huang

Posted Date: 14 August 2025

doi: 10.20944/preprints202508.1046.v1

Keywords: Landau levels; magnetic field behavior; magnetic properties; Dirac cone materials; flat band; dice lattice; Lieb lattice

 doi:10.20944/preprints202508.1046.v1

Article

Landau Levels and Electronic States for Pseudospin-1 Lattices with a Bandgap: Application to a Lieb Lattice

Liubov Zhemchuzhna [1,2,3,*] Lovely Joseph [1], Andrii Iurov [1,*] Godfrey Gumbs [3,4] and Danhong Huang [5]

[1] Department of Physics and Computer Science, Medgar Evers College of City University of New York, Brooklyn, NY 11225, USA
[2] Department of Physics & Engineering Physics, Fordham University, Bronx, NY 10458, USA
[3] Department of Physics and Astronomy, Hunter College of the City University of New York, 695 Park Avenue, New York, New York 10065, USA
[4] Donostia International Physics Center (DIPC), P de Manuel Lardizabal, 4, 20018 San Sebastian, Basque Country, Spain
[5] Space Vehicles Directorate, US Air Force Research Laboratory, Kirtland Air Force Base, New Mexico 87117, USA
* Correspondence: lzhemchuzhna@mec.cuny.edu or lzhemchuzhna@fordham.edu (L.Z.); aiurov@mec.cuny.edu or theorist.physics@gmail.com (A.I.)

Abstract

We have carried out detailed theoretical and numerical calculations, and developed a physics-based model for quantitatively describing the Landau levels of several pseudospin-1 structures with a flat band and a finite bandgap in their electronic-energy spectrum under a strong and uniform magnetic field. We have investigated the Landau-level based dynamics, as well as the corresponding eigenstates, for gapped graphene, a dice lattice with both zero and finite bandgap, and, eventually, for the Lieb lattice acquiring an asymmetric elevated flat band. Exact analytical consideration of Landau-level states has been performed and explained when dealing with all types of considered lattices. Our model could be further generalized for treating the case with an arbitrary position for the flat band between the valence and conduction bands. Our current results have direct implications for a deep-level investigation of the quantum Hall effect, as well as other magnetic and topological properties of these novel materials.

Keywords: Landau levels; magnetic field behavior; magnetic properties; Dirac cone materials; flat band; dice lattice; Lieb lattice

1. Introduction

Since the ground breaking transport measurements were reported on graphene in 2004, [1] all the novel low-dimensional materials have received tremendous attention from researchers in condensed matter physics and relevant materials science fields. Later, some other structures with tunable spin-orbit bandgaps, such as buckled honeycomb lattices, were discovered. Their magneto-optical properties [2] were also studied thoroughly, including general collective-excitation modes [3–10] and massive hyperbolic plasmons [11]. Furthermore, other novel electron dispersions have been founded in both Kekule-distorted graphene [12–15] and semi-Dirac materials. Meanwhile, their optical properties [16,17] and topological electronic behaviors [18] were investigated extensively. Specifically, the optical conductivity of all these materials, [14,19–21] including anisotropic and tilted [22] Dirac cones, [23–26] was fully explored both theoretically and experimentally.

Among these recently discovered two-dimensional lattices, a special attention has been put on unique materials with a flat (or nondispersive) band in their low-energy band structure. [27,28] This flat band, which could be located at arbitrary positions between an upper-conduction and a lower-valance band, leads to an infinite degeneracy for energies of these flat-band electrons and brings out new features to electronic properties of this type of materials. [29] Some typical examples of such flat-band

 doi:10.20944/preprints202508.1046.v1

materials include a dice, Lieb [30–32] and Kagome lattices [33–35], as well as few other important materials. [36,37]

The α-$\mathcal{T}_3$ model represents a very special type of two-dimensional structure which also exhibits a flat band in their low-energy spectrum. [38,39] The flat band in the α-$\mathcal{T}_3$ model originates from the existence of an additional hub atom at the center of each hexagon of a graphene-like two-dimensional lattice. The hopping coefficients between the hub and rim (regular) atoms in α-$\mathcal{T}_3$ model could be parameterized by a chosen number α within the range $0 < \alpha < 1$. Consequently, we obtain a physical model, which describes realistically a verity of materials with a flat band, and simultaneously, receives tremendous attention from researchers. Specifically, electronic structures, [40–42] transport, [43–46] collective optical, [4] magnetic, [47] electronic phenomena in α-$\mathcal{T}_3$ rings, [48,49] and properties of other two-dimensional lattice materials [29,50] have been extensively investigated.

Interestingly, the main characteristics of the electronic dispersions, such as band gaps, group velocities and anisotropy of graphene and other two-dimensional materials, will change significantly by applying an off-resonance electromagnetic dressing field. [51–54] In such a case, the modification of energy spectrum depends strongly on the polarization of incident irradiation, in addition to the field frequency and strength. In fact, there has already been a number of crucial publications aiming to study the electronic, collective and transport properties of materials with a Dirac cone deformed by an optical-dressing field. [55–57]

As a different and impactful issue, magnetic properties of these emergent two-dimensional materials and the corresponding electron dynamics under magnetic fields have also been explored extensively and received encouraging responses from researchers working in various fields. This includes the calculation and detailed analysis of Landau-level dispersion and electronic states under a magnetic field in graphene, [58–60] silicene, [61,62] and transition-metal dichalcogenides, [63,64] covering their magneto-optical [65,66] and magneto-transport [67–71] properties as well. Meanwhile, various magnetic-field responses of α-$\mathcal{T}_3$ material were also studied. [62] In addition, this research effort further extends to magneto-plasmons and other collective behaviors in graphene materials [72] with a tunable spin-orbit bandgap [2,62,73,74] and in α-$\mathcal{T}_3$model [75,76] as well.

The remaining part of this paper is organized as follows. In Sec. 2, we present general formalism for Dirac electrons in magnetic fields, including their energy eigenvalues (Landau levels) as well as their wave functions. Section 3 is devoted to presenting several novel derivations for some known results associated with Landau levels within a gapped graphene, including computing wave functions for the case with a finite gap Δ_0. In Sec. 4, we consider Landau quantization of electrons and corresponding electronic states within a dice lattice with both zero and a finite bandgap, accompanied by a flat band sitting at the middle between a valence and conduction bands. After that, we derive in Sec. 5 the Landau levels and corresponding eigenstates of electrons within a Lieb lattice with an elevated flat band. Finally, the final remarks and conclusions are drawn in Section 6.

2. General Formalism for Landau Quantization

We begin with a brief review of general mathematical formalism employed in calculating the energy eigenstats of free electrons under a spatially uniform magnetic field $\boldsymbol{B}$, usually referred to as Landau levels. We shall employ the Landau gauge for the vector potential $\boldsymbol{A} = \{A_x, A_y, A_z\}$ so that $A_x = B_0 y$ while $A_y = A_z = 0$. Therefore, the magnetic field in this case is given by $\boldsymbol{B} = \boldsymbol{\nabla} \times \boldsymbol{A} = B_0 \hat{\boldsymbol{z}}$, which is uniform in space domain.

Formally, the effect of a magnetic field $\boldsymbol{B}$ can be included by using a so-called Peierls substitution in any considered Hamiltonian, *i.e.*,

$$k_{x,y} \longrightarrow k_{x,y} + \frac{e}{\hbar} A_{x,y} \,. \tag{1}$$

In the case of graphene, its Hamiltonian operator acquires the following explicit form [77]

 doi:10.20944/preprints202508.1046.v1

$$\hat{\mathcal{H}}_g = \sqrt{2}\,\frac{\hbar v_F}{\ell_B}\begin{bmatrix} 0 & \hat{a} \\ \hat{a}^\dagger & 0 \end{bmatrix}, \tag{2}$$

where $\ell_B = \sqrt{\hbar/eB_0}$ is magnetic length, and two operators are defined by

$$\begin{aligned} \hat{a} &= \ell_B\, k_x + \frac{y}{\ell_B} + i\ell_B\, k_y\,, \\ \hat{a}^\dagger &= \ell_B\, k_x + \frac{y}{\ell_B} - i\ell_B\, k_y\,, \end{aligned} \tag{3}$$

which are known as the creation and annihilation operators, respectively. Using the expression in Equation (3), one can further verify the well-known commutation relation $\left[\hat{a}, \hat{a}^\dagger\right] = 1$, and meanwhile, obtain the results for their actions on the electronic states in the Fock space, given by

$$\begin{aligned} \hat{a}\,|n\rangle &= \sqrt{n}\,|n-1\rangle\,, \\ \hat{a}^\dagger\,|n\rangle &= \sqrt{n+1}\,|n+1\rangle\,. \end{aligned} \tag{4}$$

Here, the results in Equations (1)–(4) are all the relations required to calculate the actual Landau levels and their corresponding wave functions in Dirac-cone materials considered in this study.

3. Magneto-Energy Levels of Gapped Graphene

As a start, we consider the case of gapped graphene described by the following low-energy Hamiltonian

$$\hat{\mathcal{H}}_g^{(0)} = \hat{\Sigma}_{x,y}^{(2)} \cdot \boldsymbol{k} + \Delta_0\,\hat{\Sigma}_z^{(2)} = \begin{bmatrix} \Delta_0 & \hbar v_F(k_x - ik_y) \\ \hbar v_F(k_x + ik_y) & -\Delta_0 \end{bmatrix}, \tag{5}$$

which differs from well-known graphene by a finite gap $2\Delta_0$ included as a $\hat{\Sigma}_z^{(2)}$ term. Here, $\hat{\Sigma}_{x,y,z}^{(2)}$ are regular 2×2 Pauli matrices.

In the presence of a magnetic field $\boldsymbol{B} = B_0\hat{\boldsymbol{z}}$, the canonical substitution or Peierls substitution in Equation (1) can be emplyed, which leads to the following new Hamiltonian

$$\hat{\mathcal{H}}_g(B) = \begin{bmatrix} \Delta_0 & \gamma_B\hat{a} \\ \gamma_B\hat{a}^\dagger & -\Delta_0 \end{bmatrix}, \tag{6}$$

where $\gamma_B = \sqrt{2}\,\hbar v_F/\ell_B$. Mathematically speaking, the simplest way to find energy eigenvalues of the Hamiltonian in Equation (6) is simply taking the square on both sides of the eigenvalue equation. As a result, we get a new diagonal Hamiltonian matrix, written as

$$\hat{\mathcal{H}}_g^2(B) = 2\left(\frac{\hbar v_F}{\ell_B}\right)^2\begin{bmatrix} \gamma_B\,(\hat{a}^\dagger\hat{a}+1) + \Delta_0^2 & 0 \\ 0 & \gamma_B\,\hat{a}^\dagger\hat{a} + \Delta_0^2 \end{bmatrix}. \tag{7}$$

By using the harmonic-oscillator relation $\hat{a}^\dagger\hat{a}\,|n\rangle = n\,|n\rangle$, as well as the following eigenvalue relation

$$\hat{\mathcal{H}}_g^2|\Psi_n\rangle = \varepsilon_n^2\,|\Psi_n\rangle\,, \tag{8}$$

we immediately find $\varepsilon_n = \pm\sqrt{2n\,\gamma_B^2 + \Delta_0^2}$.

In a similar way, we will look for a solutions in the following general form

 doi:10.20944/preprints202508.1046.v1

$$|\Psi^{(G)}_{n_1,n_2}\rangle = \begin{bmatrix} c_1\,|n_1\rangle \\ \\ c_2\,|n_2\rangle \end{bmatrix}, \tag{9}$$

then the corresponding eigenvalue equations become

$$\begin{aligned} \Delta_0\, c_1\,|n_1\rangle + \gamma_B\, c_2\,\hat{a}\,|n_2\rangle &= \varepsilon\, c_1\,|n_1\rangle\,, \\ \gamma_B\, c_1\,\hat{a}^\dagger\,|n_1\rangle - \Delta_0\, c_2\,|n_2\rangle &= \varepsilon\, c_2\,|n_2\rangle\,. \end{aligned} \tag{10}$$

Equation (10) can be equivalently written as

$$\begin{aligned} \Delta_0\, c_1\,|n_1\rangle + \gamma_B\, c_2\,\sqrt{n_2}\,|n_2-1\rangle &= \varepsilon\, c_1\,|n_1\rangle\,, \\ \gamma_B\, c_1\,\sqrt{n_1+1}\,|n_1+1\rangle - \Delta_0\, c_2\,|n_2\rangle &= \varepsilon\, c_2\,|n_2\rangle\,. \end{aligned} \tag{11}$$

From Equation (11), we easily find that its solution in the Fock space exists only for $n_1 = n_2 - 1$, or equivalently $n_2 = n_1 + 1$. Now, let us assume $n_2 = n$ and $n_1 = n - 1$. By following Equation (11), we acquire

$$\begin{aligned} \Delta_0\, c_1\,|n-1\rangle + \gamma_B\, c_2\,\sqrt{n}\,|n-1\rangle &= \varepsilon\, c_1\,|n-1\rangle\,, \\ \gamma_B\, c_1\,\sqrt{n}\,|n\rangle - \Delta_0\, c_2\,|n\rangle &= \varepsilon\, c_2\,|n\rangle\,. \end{aligned} \tag{12}$$

The presence of a physical solution to Equation (12) requires that its coefficient determinant must be zero. This leads to the following dispersion relation

$$2v_F^2\, eB\hbar\, n - \varepsilon_n^2 + \Delta_0^2 = 0\,, \tag{13}$$

which produces $\varepsilon_n = \pm\sqrt{2v_F^2\, eB\hbar\, n + \Delta_0^2}$, and it is equivalent to a spectrum equation for Landau levels of a gapped graphene. Additionally, its wave function for $n \geq 1$ is found to be

$$|\Psi_n\rangle(\Delta_0) = \begin{bmatrix} \gamma_B\,\sqrt{n}\,|n-1\rangle \\ \\ \pm\Big(\sqrt{\gamma_B^2\, n + \Delta_0^2} - \Delta_0\Big)\,|n\rangle \end{bmatrix}. \tag{14}$$

If $\Delta_0 \to 0$, on the other hand, the result in Equation (14) immediately turns into

$$|\Psi_{n>0}\rangle(\Delta_0 \to 0) = \frac{1}{\sqrt{2}} \begin{bmatrix} |n-1\rangle \\ \\ \pm|n\rangle \end{bmatrix}, \tag{15}$$

which is reduced to the case for free-standing (zero-gap) graphene. In particular, for $n = 0$, the wave function (14) reduces to

$$|\Psi_{n=0}\rangle = \begin{bmatrix} 0 \\ \\ |0\rangle \end{bmatrix}. \tag{16}$$

 doi:10.20944/preprints202508.1046.v1

Up to here, we have finished the calculation for a closed-form analytical expression of both electronic states and Landau energy levels of electrons within a gapped graphene under an external perpendicular magnetic field.

4. Dice Lattice with Zero Bandgap

As we mentioned previously in this paper, our present study focuses on investigating pseudospin-1 Dirac materials having a flat band in their low-energy spectrum. The schematics of energy dispersions in both gapped dice and Lieb lattices, as depicted in Figure 1, contains a flat band, which makes these materials and their electronic properties similar to each other. Interestingly, different position of this flat band inside a bandgap results in a significant difference between the two. In the case of a gapped dice lattice, it sits exactly in the middle between the valence and conduction bands, separated equally from bandedges by a bandgap parameter Δ_0, and this makes the whole energy spectrum very symmetric. In another case, i.e., the Lieb lattice, the flat band is located at an elevated position, intersecting the bottom of a conduction band. Such an overlap of the flat band with the bottom of a conduction band has a lot of implications for collective and many-body properties for electrons in these types of materials, *e.g.*, in the computed polarization function, where all electronic transitions and various energy separations will be taken into account. Here, we focus on the role which the location of the flat-band plays in the presence of a perpendicular and spatially-uniform magnetic field.

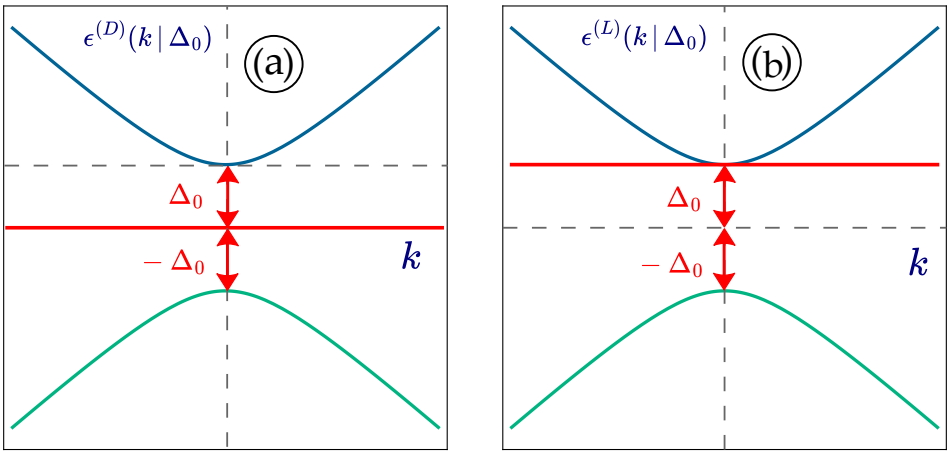

Figure 1. (Color online) Comparison of schematics for low-energy electronic dispersions $\varepsilon^{(D,L)}(k\,|\,\Delta_0)$ of a gapped dice lattice (D, left) and a Lieb lattice (L, right). The common feature for two materials is the presence of three energy bands, including one dispersionless flat band. However, the relative position of the flat band is quite different for these two lattices. In the left panel for a dice lattice, the flat band sits exactly in the middle between a valence and conduction bands, leading to additional symmetry in this band structure. However, the flat band of a Lieb lattice in the right panel locates at an elevated position intersecting with a conduction band at its lowest point.

The low-energy Hamiltonian for a dice lattice with a zero-gap parameter $\Delta_0 = 0$ (an actual bandgap is $2\Delta_0$) can be written as

$$\hat{\mathcal{H}}^{(D)}(k) = \frac{\hbar v_F}{\sqrt{2}} \begin{bmatrix} 0 & k\mathrm{e}^{-i\Theta_{\mathbf{k}}} & 0 \\ k\mathrm{e}^{i\Theta_{\mathbf{k}}} & 0 & k\mathrm{e}^{-i\Theta_{\mathbf{k}}} \\ 0 & k\mathrm{e}^{i\Theta_{\mathbf{k}}} & 0 \end{bmatrix}. \tag{17}$$

However, in the presence of a magnetic field, the Hamiltonian in Equation (17) is reansformed into

$$\hat{\mathcal{H}}^{(D)}(k) = \gamma_B^{(D)} \begin{bmatrix} 0 & \hat{a} & 0 \\ \hat{a}^\dagger & 0 & \hat{a} \\ 0 & \hat{a}^\dagger & 0 \end{bmatrix}, \tag{18}$$

 doi:10.20944/preprints202508.1046.v1

where $\hat{a}$ and $\hat{a}^\dagger$ represent annihilation and creation operators, respectively, and $\gamma_B^{(D)} = \gamma_B^{(G)}/\sqrt{2} = \hbar v_F/\ell_B$. From now on, we will calculate the energy levels (Landau levels) of a dice lattice in cases with a zero bandgap $\Delta_0 = 0$.

Here, we first write down the wave function in the most general form as

$$|\Psi_{n_1,n_2,n_3}^{(D)}\rangle = \begin{bmatrix} c_1\,|n_1\rangle \\ c_2\,|n_2\rangle \\ c_3\,|n_3\rangle \end{bmatrix}, \tag{19}$$

where c_1, c_2, c_3 are three coefficients to be determined. Inserting the wave function in Equation (19) into a Schrödinger equation with its Hamiltonian given by Equation (18), one finds an eigenvalue equation as follows:

$$\begin{aligned} &\gamma_B^{(D)}\,\hat{a}\,c_2|n_2\rangle - \varepsilon\,c_1\,|n_1\rangle = 0\,, \\ &\gamma_B^{(D)}\,\hat{a}^\dagger\,c_1|n_1\rangle + \gamma_B\,\hat{a}\,c_3\,|n_3\rangle - \varepsilon\,c_2\,|n_2\rangle = 0\,, \\ &\gamma_B^{(D)}\,\hat{a}^\dagger\,c_2|n_2\rangle - \varepsilon\,c_3\,|n_3\rangle = 0\,, \end{aligned} \tag{20}$$

where parameter ε stands for the eigenvalue to be determined. After analyzing Equation (20), we know that the conditions of $n_1 = n_2 - 1$ and $n_2 = n_3 - 1$ must be satisfied in order to acquire a nonzero (non-trivial) solution of these coupled equations. Specifically, by writing $n_3 = n$, $n_2 = n-1$ and $n_1 = n-2$, we find from Equation (20) that

$$\begin{aligned} &-\varepsilon\,c_1 + \gamma_B^{(D)}\,\sqrt{n-1}\,c_2 = 0\,, \\ &\gamma_B^{(D)}\,\sqrt{n-1}\,c_1 - \varepsilon\,c_2 + \gamma_B^{(D)}\,\sqrt{n}\,c_3 = 0\,, \\ &\gamma_B^{(D)}\,\sqrt{n}\,c_2 - \varepsilon\,c_3 = 0\,. \end{aligned} \tag{21}$$

After an analysis of Equation (21), it becomes clear that this system could support nonzero solution $[c_1,\, c_2,\, c_3]^T \neq 0$ only if its coefficient determinant is zero. In this way, we find the energy dispersions of a dice lattice, given by $\varepsilon_n = 0$ for a flat band, as well as by another nonzero solution

$$\varepsilon_n = \pm\gamma_B^{(D)}\sqrt{2n-1}\,. \tag{22}$$

The solved wave functions associated with Equation (22) are

$$|\Psi_n^{(D)}\rangle = \frac{1}{\sqrt{2(2n-1)}} \begin{bmatrix} \sqrt{n-1}\,|n-2\rangle \\ \pm\,|n-1\rangle \\ \sqrt{n}\,|n\rangle \end{bmatrix}, \tag{23}$$

where $n = 1,\, 2,\, 3,\, \cdots$. By choosing $n = 1$ in Equation (23) as an example, we have

$$|\Psi_{n=1}^{(D)}\rangle = \frac{1}{\sqrt{2}} \begin{bmatrix} 0 \\ \pm|0\rangle \\ |1\rangle \end{bmatrix}. \tag{24}$$

For the flat band $\varepsilon_n = 0$, on the other hand, its wave function is

$$|\Psi_n^{(D)}\rangle = \frac{1}{\sqrt{(2n-1)}} \begin{bmatrix} \sqrt{n}\,|n-2\rangle \\ 0 \\ -\sqrt{n-1}\,|n\rangle \end{bmatrix}, \tag{25}$$

where $n = 2, 3, 4, \ldots$. However, as $n = 1$, the wave function is modified to

 doi:10.20944/preprints202508.1046.v1

$$|\Psi^{(D)}_{n=1}\rangle = \frac{1}{\sqrt{2}} \begin{bmatrix} 0 \\ 0 \\ -|0\rangle \end{bmatrix}. \tag{26}$$

The Landau levels for a zero-bandgap dice lattice, as shown in Figure 2, is actually a specific limiting case of the energy eigenstates of α-$\mathcal{T}_3$ materials, which was discussed in Ref. [47]. In the presence of a magnetic field, the eigen-energies of valence and conduction bands reduces to an infinite set of quantized energy levels $\backsim \pm\sqrt{2n-1}$, but the flat band $\varepsilon_n = 0$ remains dispersionless with an infinite degeneracy. Consequently, we conclude that such configuration of Landau levels displays both similarities and distinctions (a constant energy shift) in comparison with energy dispersion $\varepsilon_n \backsim \sqrt{2n}$ of graphene.

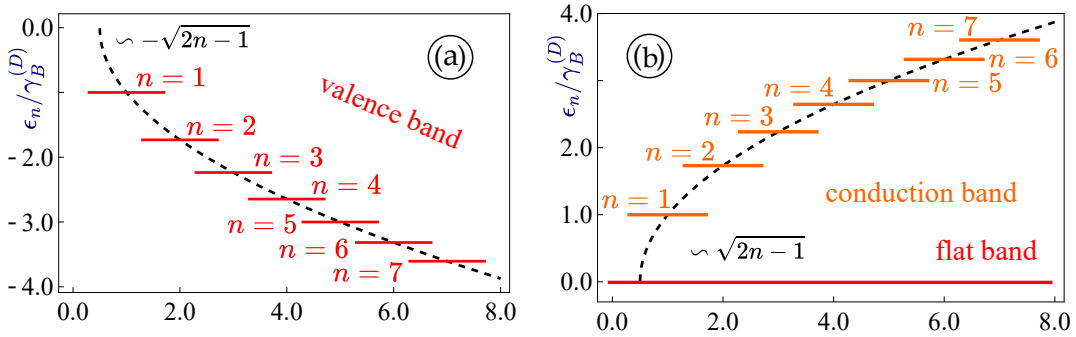

Figure 2. (Color online) Calculated scaled Landau levels $\varepsilon_n/\gamma_B^{(D)}$ as a function of level index n for a zero-gap ($\Delta_0 = 0$) dice lattice: the scaled energy levels $\varepsilon_n/\gamma_B^{(D)}$ of a dice lattice with $\Delta_0 = 0$ under a uniform magnetic field are obtained from analytical expressions in Equation (22). Here, the flat band (*i.e.*,, the long-red line at the bottom of right panel) corresponds to a set of degenerate Landau levels $\varepsilon_n = 0$. As labeled, the dashed curves in two panels show two functions $\pm\sqrt{2n-1}$ for the left (valence band, $-$) and the right (conduction band, $+$) panels, respectively.

5. Gapped Dice Lattice

A dice lattice with a finite bandgap Δ_0 is obtained in terms of a 3×3 generalization of the Pauli matrices $\hat{\Sigma}^{(3)}_{x,y,z}$ in the following way:

$$\hat{\mathcal{H}}^{(D)}(k) = \hat{\Sigma}^{(3)}_{x,y} \cdot \boldsymbol{k} + \Delta_0 \hat{\Sigma}^{(3)}_z = \frac{\hbar v_F}{\sqrt{2}} \begin{bmatrix} \Delta_0 & k\mathrm{e}^{-i\Theta_{\mathbf{k}}} & 0 \\ k\mathrm{e}^{i\Theta_{\mathbf{k}}} & 0 & k\mathrm{e}^{-i\Theta_{\mathbf{k}}} \\ 0 & k\mathrm{e}^{i\Theta_{\mathbf{k}}} & -\Delta_0 \end{bmatrix}, \tag{27}$$

where

$$\hat{\Sigma}^{(3)}_x = \begin{bmatrix} 0 & 1 & 0 \\ 1 & 0 & 1 \\ 0 & 1 & 0 \end{bmatrix}, \tag{28}$$

$$\hat{\Sigma}^{(3)}_y = \begin{bmatrix} 0 & -i & 0 \\ i & 0 & -i \\ 0 & i & 0 \end{bmatrix}, \tag{29}$$

which are supplemented by an extra bandgap-related matrix, *i.e.*,

$$\hat{\Sigma}^{(3)}_z = \begin{bmatrix} 1 & 0 & 0 \\ 0 & 0 & 0 \\ 0 & 0 & -1 \end{bmatrix}. \tag{30}$$

In the presence of a magnetic field, the Hamiltonian in Equation (27) is transformed into the form similar to the expression in Equation (18), and written as

 doi:10.20944/preprints202508.1046.v1

$$\hat{\mathcal{H}}^{(D)}(k) = \gamma_B^{(D)} \begin{bmatrix} \Delta_0 & \hat{a}^\dagger & 0 \\ \hat{a}^\dagger & 0 & \hat{a} \\ 0 & \hat{a}^\dagger & -\Delta_0 \end{bmatrix}. \tag{31}$$

In correspondence with Equation (21) having $\Delta_0 = 0$, for current case, we find

$$\begin{aligned} &-(\Delta_0 + \varepsilon)\, c_1 + \gamma_B^{(D)} \sqrt{n-1}\, c_2 = 0 \\ &\gamma_B^{(D)} \sqrt{n-1}\, c_1 - \varepsilon\, c_2 + \gamma_B^{(D)} \sqrt{n}\, c_3 = 0 \\ &\gamma_B^{(D)} \sqrt{n}\, c_2 + (\Delta_0 - \varepsilon)\, c_3 = 0\,. \end{aligned} \tag{32}$$

Compared with the case of $\Delta_0 = 0$, the finite value of Δ_0 here results in a quite different asymmetric dispersion equation, *i.e.*,

$$\left(\gamma_B^{(D)}\right)^2 \Delta_0 - \left(\gamma_B^{(D)}\right)^2 \varepsilon_n + 2n \left(\gamma_B^{(D)}\right)^2 \varepsilon_n + \Delta_0^2\, \varepsilon_n - \varepsilon_n^3 = 0\,, \tag{33}$$

which cannot be solved in any straightforward way. However, by utilizing an analogy to a trigonometrical expansion formula, as discussed in Refs. [78] and [42], it can also be solved by using a perturbation approach as follows:

$$\varepsilon_n = \varepsilon_n^{(0)} + \varepsilon_n^{(1)}\, \Delta_0 + \varepsilon_n^{(2)}\, \Delta_0^2 + \cdots\,, \tag{34}$$

where the bandgap Δ_0 is regarded as a small parameter for this expansion. Interestingly, for the flat band with $\varepsilon_n^{(0)} = 0$, one obtains $\varepsilon_n^{(1)} = -1/(2n-1)$, and thus

$$\varepsilon_n = \frac{-\Delta_0}{2n-1}\,. \tag{35}$$

We have obtained numerically a set of discrete Landau levels which are presented in Figure 3. We first notice that the valence and conduction bands are not exactly symmetric with respect to zero energy and no simple analytical formula or approximate expression exists for describing energy locations of these levels. For the high-energy states with $n \gg 1$, the energy eigenstates are well approximated by expressions $\backsim \pm\sqrt{2n-1}$, implying that the effect due to bandgap Δ_0 is decreased. This further supports the validity of a simple but efficient application of the WKB approximation for this case. Here, the flat band is no longer dispersionless and its degeneracy is lifted. On the other hand, we find an infinite set of separated non-dengenerate Landau levels within a negative-energy $\varepsilon_n < 0$ region. For large $n \gg 1$, the effect of an energy gap becomes negligible and these levels approach the $\varepsilon_n = 0$ level.

Next, we focus on the dependence of energy levels for a gapped dice lattice on the gap parameter Δ_0, and present various numerically computed results in Figure 4 for a full comparison among Landau levels in the conduction, valence and flat bands all together. As found from Figure 4, these numerical results once again agree with our previous findings that the high-energy Landau levels with large level index n ($n \gg 1$) will be much less sensitive to the size of bandgap Δ_0, which can be easily verified by the fact that large-n Landau levels would like to group together as Δ_0 increases for the flat-band case. In particular, the $n = 1$ Landau level in panel (b) demonstrates a negative linear dependence on Δ_0, which fully agrees with our perturbation-based solution in Equation (35).

 doi:10.20944/preprints202508.1046.v1

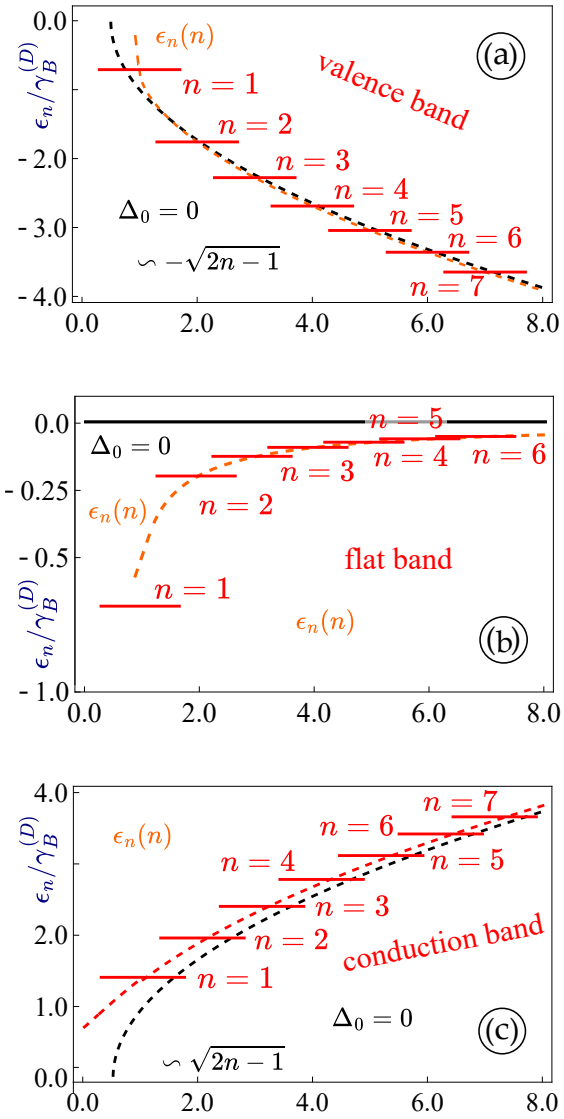

Figure 3. (Color online) The scaled Landau levels $\varepsilon_n/\gamma_B^{(D)}$ as a function of level index n for a finite-gap dice lattice: the energy eigenstates of a dice lattice with a finite bandgap $\Delta_0 = 0.7\,\gamma_B^{(D)}$ under a uniform magnetic field, which are calculated by using Equation (35). As labeled, three panels (a), (b) and (c) represent the energy levels of the valence, flat and conduction bands, separately. The flat band (long-black line at the top of panel (b)) splits into a set of non-equidistant Landau levels with a lifted degeneracy depending on bandgap Δ_0.

 doi:10.20944/preprints202508.1046.v1

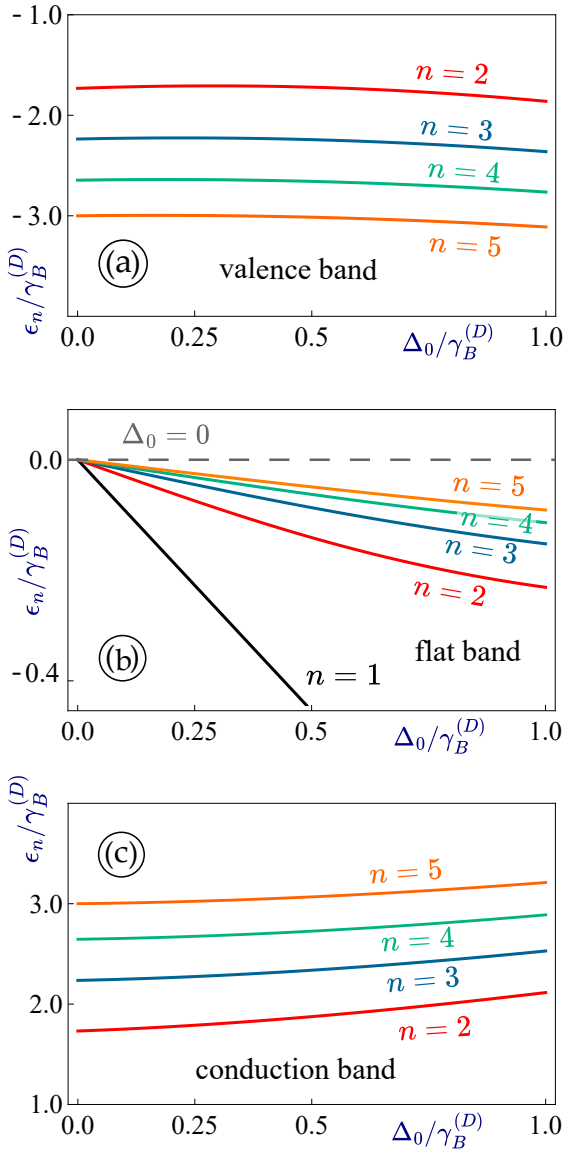

Figure 4. (Color online) The scaled Landau levels $\varepsilon_n/\gamma_B^{(D)}$ of a finite-gap dice lattice as a function of the scaled energy bandgap $\Delta_0/\gamma_B^{(D)}$ for a gapped dice lattice under a uniform magnetic field, which are obtained by numerically solving the root ε_n of Equation (33). As labeled, three panels (a), (b) and (c) display the dependence of Landau levels on $\Delta_0/\gamma_B^{(D)}$ for valence, flat and conductione bands, respectively. The flat band case in panel (b) reveals a set of non-equivalent Landau levels with a lifted degeneracy depending on Δ_0. Here, the bandgap in panels (a) and (c) is chosen as $\Delta_0 = 0.7\,\gamma_B^{(D)}$.

6. Modeling Lieb Lattice with Elevated Flat Band

we now turn our attention to the major issue of this paper, *i.e.*,, modeling the effect of a magnetic field on a Lieb lattice with a non-symmetric elevated flat band, as depicted in Figure 1(b). In this case, the low-energy Hamiltonian is found to be [26]

$$\hat{\mathcal{H}}^{(L)}(\boldsymbol{k}\,|\,k_\Delta) = \hbar v_F \begin{bmatrix} k_\Delta & k_x & 0 \\ k_x & -k_\Delta & k_y \\ 0 & k_y & k_\Delta \end{bmatrix}, \tag{36}$$

where the following substitution

$$k_{x,y} \to \frac{\pi}{a_0} + k_{x,y} \tag{37}$$

 doi:10.20944/preprints202508.1046.v1

is required for a Lieb lattice, and a_0 stands for the lattice parameter. Here, before putting the substitution in Equation (37) into Equation (36), three energy dispersions can be easily found from the Hamiltonian in Equation (36) as $\varepsilon^{(L)}_{\gamma=\pm1}(\boldsymbol{k}\,|\,k_\Delta)/\hbar v_F = \gamma\sqrt{k_\Delta^2+k_x^2+k_y^2}$ and $\varepsilon^{(L)}_{\gamma=0}(\boldsymbol{k}\,|\,k_\Delta)/\hbar v_F = k_\Delta$, which could be combined into a single expression, yielding

$$\varepsilon^{(L)}_{\gamma}(\boldsymbol{k}\,|\,k_\Delta) = \hbar v_F\left[\delta_{\gamma,0}\,k_\Delta + \gamma\,(1-\delta_{\gamma,0})\,\sqrt{k_\Delta^2+k^2}\right], \tag{38}$$

where $\gamma = 0, \pm1$, and $\delta_{\gamma,0}$ is the Kronecker symbol.

In the presence of a magnetic field, however, the Hamiltonian in Equation (36) will change into

$$\hat{\mathcal{H}}^{(L)}(\boldsymbol{k}\,|\,k_\Delta) = \begin{bmatrix} \Delta_0 & \frac{\gamma^{(L)}_B}{\sqrt{2}}\left(\hat{a}+\hat{a}^\dagger\right) & 0 \\ \frac{\gamma^{(L)}_B}{\sqrt{2}}\left(\hat{a}+\hat{a}^\dagger\right) & -\Delta_0 & \frac{\gamma^{(L)}_B}{\sqrt{2}i}\left(\hat{a}-\hat{a}^\dagger\right) \\ 0 & \frac{\gamma^{(L)}_B}{\sqrt{2}i}\left(\hat{a}-\hat{a}^\dagger\right) & \Delta_0 \end{bmatrix}. \tag{39}$$

Here, it is straightforward to verify that one cannot project this Hamiltonian onto the same Fock-state $|n\rangle$ representation. However, by searching for the eigen-function in terms of Equation (39), we obtain one of its eigenvalue equations, given by

$$\Delta_0\,c_1\,|n_1\rangle + \frac{\gamma^{(L)}_B}{\sqrt{2}}\left[\sqrt{n_2}\,c_2\,|n_2-1\rangle + \sqrt{n_2+1}\,c_2\,|n_2+1\rangle\right] = \varepsilon_n\,c_1\,|n_1\rangle\,. \tag{40}$$

Unfortunately, Equation (40) cannot be satisfied by any $|n_1\rangle$ and $|n_2\rangle$ states.

On the other hand, we are also able to model the Lieb lattice by an elevated flat band, as illustrated in Figure 1. For this purpose, let us first write down the Hamiltonian, by using an elevated flat band, as

$$\hat{\mathcal{H}}^{(L)}(\boldsymbol{k}) = \begin{bmatrix} \Delta_0 & \frac{\gamma^{(L)}_B k}{\sqrt{2}}\mathrm{e}^{-i\Theta_{\mathbf{k}}} & 0 \\ \frac{\gamma^{(L)}_B k}{\sqrt{2}}\mathrm{e}^{i\Theta_{\mathbf{k}}} & -\Delta_0 & \frac{\gamma^{(L)}_B k}{\sqrt{2}}\mathrm{e}^{-i\Theta_{\mathbf{k}}} \\ 0 & \frac{\gamma^{(L)}_B k}{\sqrt{2}}\mathrm{e}^{i\Theta_{\mathbf{k}}} & \Delta_0 \end{bmatrix}, \tag{41}$$

which results in two energy dispersions, given by $\varepsilon^{(L)}_{\gamma}(k) = \Delta_0$ as well as $\varepsilon^{(L)}_{\gamma}(k) = \gamma\sqrt{k^2+\Delta_0^2}$. Furthermore, in the presence of a magnetic field, we find that the Hamiltonian in Equation (39) changes into

$$\hat{\mathcal{H}}^{(L)}(k) = \gamma^{(L)}_B\begin{bmatrix} \Delta_0 & \hat{a} & 0 \\ \hat{a} & -\Delta_0 & \hat{a}^\dagger \\ 0 & \hat{a}^\dagger & \Delta_0 \end{bmatrix}. \tag{42}$$

Correspondingly, previous Equation (21) for a dice lattice will be changed into

$$\begin{aligned} &(\Delta_0-\varepsilon)\,c_1 + \gamma^{(L)}_B\sqrt{n-1}\,c_2 = 0\,, \\ &\gamma^{(L)}_B\sqrt{n-1}\,c_1 - (\Delta_0+\varepsilon)\,c_2 + \gamma^{(D)}_B\sqrt{n}\,c_3 = 0\,, \\ &\gamma^{(L)}_B\sqrt{n}\,c_2 + (\Delta_0-\varepsilon)\,c_3 = 0\,. \end{aligned} \tag{43}$$

Equation (43) leads to the eigen-value equation as

$$\left(\gamma^{(L)}_B\right)^2\Delta_0 - 2n\left(\gamma^{(L)}_B\right)^2\Delta_0 - \Delta_0^3 - \left(\gamma^{(L)}_B\right)^2\varepsilon_n + 2n\left(\gamma^{(L)}_B\right)^2\varepsilon_n + \Delta_0^2\,\varepsilon_n + \Delta_0\,\varepsilon_n^2 - \varepsilon_n^3 = 0\,, \tag{44}$$

which gives rise to the energy levels by

 doi:10.20944/preprints202508.1046.v1

$$\varepsilon_n = \Delta_0 \,, \tag{45}$$

$$\varepsilon_n = \pm\sqrt{\left(\gamma_B^{(L)}\right)^2 (2n-1) + \Delta_0^2} \,. \tag{46}$$

Here, the most interesting thing is the wave function corresponding to the flat band with $\varepsilon_n = \Delta_0$. In fact, from Equation (43), we immediately conclude that $c_2 = 0$. Thus, this leaves us with

$$\sqrt{n-1}\, c_1 = -\sqrt{n}\, c_3 \,, \tag{47}$$

and the corresponding wave function is given by

$$|\Psi_n^{(\Delta_0)}\rangle = \frac{1}{\sqrt{(2n-1)}} \begin{bmatrix} \sqrt{n}\,|n-2\rangle \\ 0 \\ -\sqrt{n-1}\,|n\rangle \end{bmatrix} , \tag{48}$$

where $n = 2, 3, 4, \cdots$. For $n = 1$, especially, this wave function is taken as

$$|\Psi_{n=1}^{(\Delta_0)}\rangle = \frac{1}{\sqrt{2}} \begin{bmatrix} 0 \\ 0 \\ -|0\rangle \end{bmatrix} . \tag{49}$$

From Equations (48) and (49), we quickly find that they are identical to Equations (25) and (26) in the case of zero-gap dice lattice.

Finally, we calculate and plot the Landau levels for our model for a Lieb lattice obtained by relatively simple analytical expressions in Equations (45) and (46). Our results are presented in Figures 5 and 6. From these two figures, we find that these energy levels, corresponding to the valence and conduction bands, become symmetric now with respect to the zero energy. Similar to the previously considered case for a gapped dice lattice, the effect of an energy bandgap diminishes for higher Landau levels with $n \gg 1$. Meanwhile, the flat band remains dispersionless with a simple shift to the gap level $\varepsilon_n = \Delta_0$ and remains infinitely degenerate. The dependence of these energy levels on the gap Δ_0, as shown in Figure 6, clearly demonstrate such a linear dependence $\varepsilon_n = \Delta_0$, as well as a smooth and monotonic dependence of all energy levels, corresponding to the valence and conduction bands, on the gap parameter Δ_0.

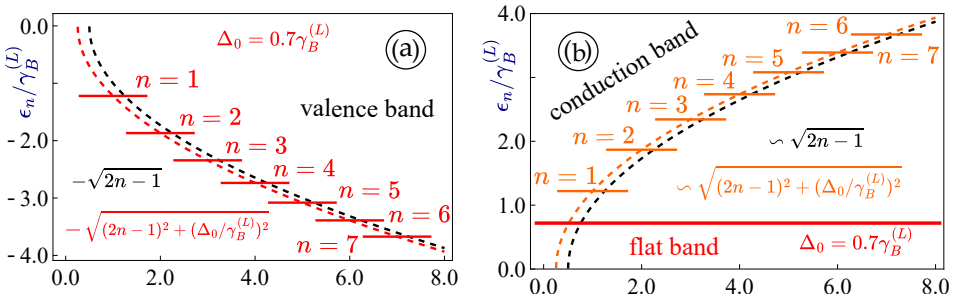

Figure 5. (Color online) Landau levels for a Lieb lattice: the energy eigenstates of a Lieb lattice with a finite bandgap $\Delta_0 = 0.7\,\gamma_B^{(D)}$ in the presence of a uniform magnetic field, and calculated from analytical expressions in Equations (45) and (46). Two panels (a) and (b) represent the energy levels corresponding to the valence (left) and conduction (right) bands, respectively.

 doi:10.20944/preprints202508.1046.v1

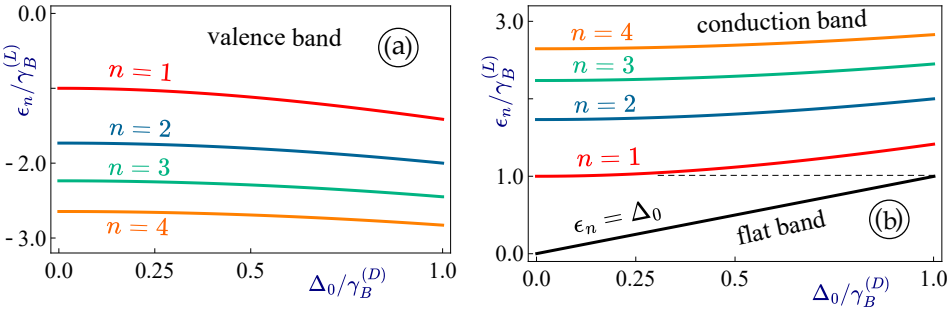

Figure 6. (Color online) Landau levels as a function of energy bandgap Δ_0 for a Lieb lattice in the presence of a uniform magnetic field, and calculated from analytical expressions in Equations (45) and (46). Two panels (a) and (b) represent the energy levels corresponding to the valence (left) and conduction (right) bands. The flat band $\varepsilon_n = \Delta_0$ in panel (b) corresponds to a set of non-equivalent Landau levels with a lifted degeneracy depending on the energy gap Δ_0.

7. Summary and Remarks

In conclusion, we note that the main thrust of this paper is to present a thorough theoretical and numerical investigation of the quantized energy levels under a uniform external magnetic field (*i.e.*,, Landau levels) and the corresponding electronic states for several important Dirac cone materials with a flat band in their low-energy spectra.

First, we considered a well-known case for graphene with an energy bandgap and provided new derivations for Landau quantization in this system, given by $\backsim \sqrt{(\hbar v_F k)^2 + \Delta_0^2}$. Surprisingly, the square Hamiltonian of graphene with a finite bandgap under a magnetic field reduces to a diagonal matrix, which immediately gives rise to the corresponding energy eigenvalues, similarly to the case of an intrinsic graphene with a zero bandgap.

Next, we investigated the electronic states under a magnetic field in a dice lattice with a finite bandgap, which is shown as a limiting case of the general α-$\mathcal{T}_3$ model. However, the presence of a finite gap turns the eigenvalue equations into a non-trivial cubic equation for computing Landau levels in this system. This cubic equation could be solved either numerically or by using an analogy between this expression and a well-known trigonometric equation, or even a perturbation theory for a small bandgap parameter Δ_0. The result is in stark contrast with regular energy dispersions (in the absence of a magnetic field), which could be easily found from a simple algebraic equation.

Finally, we investigated the Landau levels for a realistic model of a Lieb lattice with an elevated flat band intersecting the conduction band at its lowest point. This model has both common features and differences from the dice lattice and the α-$\mathcal{T}_3$ model. The main interest on such physics models is the presence of a flat band within the bandgap region, which greatly affects the electronic, magnetic and collective properties of the material. More importantly, the location of this flat band can be quite unique for the Lieb lattice, which results in substantially reduced symmetry of its low-energy spectrum. We have calculated the Landau levels of this type of energy dispersions and obtained a relatively simple analytical result $\backsim \sqrt{2n\left(\gamma_B^{(L)}\right)^2 + \Delta_0^2}$, which provides a quantitative description for its dynamical feature under a quantizing magnetic field. Meanwhile, we have also calculated the wave function corresponding to the flat band and compared its similarity with other wave functions in a dice lattice.

Generally speaking, magnetic quantization as well as electronic and collective properties under a strong magnetic field, including magneto-transport and magneto-plasmon properties, are crucial for understanding the fundamental physics of any new material, such as quantum-Hall effect. The exact knowledge of the electronic states, discrete energy level or energy bands, is an important step in predicting or understanding their novel electronic and topological properties. Our theoretical model, novel closed-form analytical expressions and numerical results are believed to become a crucial advancement in developing next-level novel electronic nanodevices.

 doi:10.20944/preprints202508.1046.v1

Acknowledgments: A.I. was supported by the funding received from TradB-56-75, PSC-CUNY Award # 68386-00 56. G.G. gratefully acknowledges funding from the U.S. National Aeronautics and Space Administration (NASA) via the NASA-Hunter College Center for Advanced Energy Storage for Space under cooperative agreement 80NSSC24M0177. D.H. would like to acknowledge the Air Force Office of Scientific Research (AFOSR) and the views expressed are those of the authors and do not reflect the official guidance or position of the United States Government, the Department of Defense or of the United States Air Force.

References

1. Geim, A.K.; Novoselov, K.S. The rise of graphene. *Nature materials* **2007**, *6*, 183–191.
2. Tabert, C.J.; Nicol, E.J. Valley-spin polarization in the magneto-optical response of silicene and other similar 2D crystals. *Physical Review Letters* **2013**, *110*, 197402.
3. Malcolm, J.; Nicol, E. Frequency-dependent polarizability, plasmons, and screening in the two-dimensional pseudospin-1 dice lattice. *Physical Review B* **2016**, *93*, 165433.
4. Iurov, A.; Zhemchuzhna, L.; Gumbs, G.; Huang, D.; Fekete, P.; Anwar, F.; Dahal, D.; Weekes, N. Tailoring plasmon excitations in α-T 3 armchair nanoribbons. *Scientific reports* **2021**, *11*, 20577.
5. Apalkov, V.; Wang, X.F.; Chakraborty, T. Collective excitations of Dirac electrons in graphene. *International Journal of Modern Physics B* **2007**, *21*, 1165–1179.
6. Gumbs, G.; Balassis, A.; Iurov, A.; Fekete, P. Strongly localized image states of spherical graphitic particles. *The Scientific World Journal* **2014**, *2014*, 726303.
7. Guinea, F.; Le Doussal, P.; Wiese, K.J. Collective excitations in a large-d model for graphene. *Physical Review B* **2014**, *89*, 125428.
8. Gumbs, G.; Iurov, A.; Huang, D.; Pan, W. Tunable surface plasmon instability leading to emission of radiation. *Journal of Applied Physics* **2015**, *118*.
9. Rodin, A.; Trushin, M.; Carvalho, A.; Castro Neto, A. Collective excitations in 2D materials. *Nature Reviews Physics* **2020**, *2*, 524–537.
10. Gumbs, G.; Iurov, A.; Horing, N. Nonlocal plasma spectrum of graphene interacting with a thick conductor. *Physical Review B* **2015**, *91*, 235416.
11. Mojarro, M.; Carrillo-Bastos, R.; Maytorena, J.A. Hyperbolic plasmons in massive tilted two-dimensional Dirac materials. *Physical Review B* **2022**, *105*, L201408.
12. Andrade, E.; Carrillo-Bastos, R.; Naumis, G.G. Valley engineering by strain in Kekulé-distorted graphene. *Physical Review B* **2019**, *99*, 035411.
13. Andrade, E.; Carrillo-Bastos, R.; Naumis, G.G. Topical Review: Electronic and optical properties ofKekul´ e and other short wavelength spatialmodulated textures of graphene. *Journal of Physics: Condensed Matter* **2025**.
14. Herrera, S.A.; Naumis, G.G. Electronic and optical conductivity of kekulé-patterned graphene: Intravalley and intervalley transport. *Physical Review B* **2020**, *101*, 205413.
15. Iurov, A.; Zhemchuzhna, L.; Gumbs, G.; Huang, D. Application of the WKB theory to investigate electron tunneling in Kek-Y graphene. *Applied Sciences* **2023**, *13*, 6095.
16. Carbotte, J.; Bryenton, K.; Nicol, E. Optical properties of a semi-Dirac material. *Physical Review B* **2019**, *99*, 115406.
17. Mojarro, M.; Carrillo-Bastos, R.; Maytorena, J.A. Optical properties of massive anisotropic tilted Dirac systems. *Physical Review B* **2021**, *103*, 165415.
18. Mondal, S.; Ganguly, S.; Basu, S. Topology and applications of 2D Dirac and semi-Dirac materials. *Physical Sciences Reviews* **2022**.
19. Xiong, Q.Y.; Ba, J.Y.; Duan, H.J.; Deng, M.X.; Wang, Y.M.; Wang, R.Q. Optical conductivity and polarization rotation of type-II semi-Dirac materials. *Physical Review B* **2023**, *107*, 155150.
20. Stauber, T.; San-Jose, P.; Brey, L. Optical conductivity, Drude weight and plasmons in twisted graphene bilayers. *New Journal of Physics* **2013**, *15*, 113050.
21. Dey, B.; Ghosh, T.K. Dynamical polarization, optical conductivity and plasmon mode of a linear triple component fermionic system. *Journal of Physics: Condensed Matter* **2022**, *34*, 255701.
22. Mojarro, M.; Carrillo-Bastos, R.; Maytorena, J.A. Thermal difference reflectivity of tilted two-dimensional Dirac materials. *Physical Review B* **2023**, *108*, L161401.
23. Tan, C.Y.; Yan, C.X.; Zhao, Y.H.; Guo, H.; Chang, H.R.; et al. Anisotropic longitudinal optical conductivities of tilted Dirac bands in 1 T′- Mo S 2. *Physical Review B* **2021**, *103*, 125425.
24. Wild, A.; Mariani, E.; Portnoi, M.E. Optical absorption in two-dimensional materials with tilted Dirac cones. *Physical Review B* **2022**, *105*, 205306.

 doi:10.20944/preprints202508.1046.v1

25. Iurov, A.; Zhemchuzhna, L.; Gumbs, G.; Huang, D. Optical conductivity of gapped α-T 3 materials with a deformed flat band. *Physical Review B* **2023**, *107*, 195137.
26. Oriekhov, D.; Gusynin, V. Optical conductivity of semi-Dirac and pseudospin-1 models: Zitterbewegung approach. *Physical Review B* **2022**, *106*, 115143.
27. Regnault, N.; Xu, Y.; Li, M.R.; Ma, D.S.; Jovanovic, M.; Yazdani, A.; Parkin, S.S.; Felser, C.; Schoop, L.M.; Ong, N.P.; et al. Catalogue of flat-band stoichiometric materials. *Nature* **2022**, *603*, 824–828.
28. Hase, I.; Yanagisawa, T.; Kawashima, K. Computational design of flat-band material. *Nanoscale research letters* **2018**, *13*, 63.
29. Checkelsky, J.G.; Bernevig, B.A.; Coleman, P.; Si, Q.; Paschen, S. Flat bands, strange metals and the Kondo effect. *Nature Reviews Materials* **2024**, *9*, 509–526.
30. Slot, M.R.; Gardenier, T.S.; Jacobse, P.H.; Van Miert, G.C.; Kempkes, S.N.; Zevenhuizen, S.J.; Smith, C.M.; Vanmaekelbergh, D.; Swart, I. Experimental realization and characterization of an electronic Lieb lattice. *Nature physics* **2017**, *13*, 672–676.
31. Mukherjee, S.; Spracklen, A.; Choudhury, D.; Goldman, N.; Ohberg, P.; Andersson, E.; Thomson, R.R. Observation of a localized flat-band state in a photonic Lieb lattice. *Physical review letters* **2015**, *114*, 245504.
32. Qiu, W.X.; Li, S.; Gao, J.H.; Zhou, Y.; Zhang, F.C. Designing an artificial Lieb lattice on a metal surface. *Physical Review B* **2016**, *94*, 241409.
33. Lee, J.H.; Kim, G.W.; Song, I.; Kim, Y.; Lee, Y.; Yoo, S.J.; Cho, D.Y.; Rhim, J.W.; Jung, J.; Kim, G.; et al. Atomically Thin Two-Dimensional Kagome Flat Band on the Silicon Surface. *ACS nano* **2024**.
34. Guo, H.M.; Franz, M. Topological insulator on the kagome lattice. *Physical Review B—Condensed Matter and Materials Physics* **2009**, *80*, 113102.
35. Wang, Q.; Lei, H.; Qi, Y.; Felser, C. Topological quantum materials with kagome lattice. *Accounts of Materials Research* **2024**, *5*, 786–796.
36. Tang, L.; Song, D.; Xia, S.; Xia, S.; Ma, J.; Yan, W.; Hu, Y.; Xu, J.; Leykam, D.; Chen, Z. Photonic flat-band lattices and unconventional light localization. *Nanophotonics* **2020**, *9*, 1161–1176.
37. Nishino, S.; Goda, M. Three-dimensional flat-band models. *Journal of the Physical Society of Japan* **2005**, *74*, 393–400.
38. Raoux, A.; Morigi, M.; Fuchs, J.N.; Piéchon, F.; Montambaux, G. From dia-to paramagnetic orbital susceptibility of massless fermions. *Physical review letters* **2014**, *112*, 026402.
39. Illes, E. Properties of the α-T3 Model. PhD thesis, University of Guelph, 2017.
40. Iurov, A.; Gumbs, G.; Huang, D. Peculiar electronic states, symmetries, and berry phases in irradiated α- t 3 materials. *Physical Review B* **2019**, *99*, 205135.
41. Tamang, L.; Biswas, T. Probing topological signatures in an optically driven α- T 3 lattice. *Physical Review B* **2023**, *107*, 085408.
42. Dey, B.; Ghosh, T.K. Floquet topological phase transition in the α-T 3 lattice. *Physical Review B* **2019**, *99*, 205429.
43. Iurov, A.; Zhemchuzhna, L.; Fekete, P.; Gumbs, G.; Huang, D. Klein tunneling of optically tunable Dirac particles with elliptical dispersions. *Physical Review Research* **2020**, *2*, 043245.
44. Illes, E.; Nicol, E. Klein tunneling in the α- T 3 model. *Physical Review B* **2017**, *95*, 235432.
45. Ding, Z.; Wang, D.; Li, M.; Tao, Y.; Wang, J. Spin-resolved and charge Josephson diode effects in α-T 3 lattice junctions. *Physical Review B* **2024**, *110*, 155405.
46. Iurov, A.; Zhemchuzhna, L.; Dahal, D.; Gumbs, G.; Huang, D. Quantum-statistical theory for laser-tuned transport and optical conductivities of dressed electrons in α- T 3 materials. *Physical Review B* **2020**, *101*, 035129.
47. Illes, E.; Nicol, E. Magnetic properties of the α-T 3 model: Magneto-optical conductivity and the Hofstadter butterfly. *Physical Review B* **2016**, *94*, 125435.
48. Islam, M.; Biswas, T.; Basu, S. Effect of magnetic field on the electronic properties of an α- T 3 ring. *Physical Review B* **2023**, *108*, 085423.
49. Islam, M.; Basu, S. Spin and charge persistent currents in a Kane Mele α-T3 quantum ring. *Journal of Physics: Condensed Matter* **2023**.
50. Leykam, D.; Andreanov, A.; Flach, S. Artificial flat band systems: from lattice models to experiments. *Advances in Physics: X* **2018**, *3*, 1473052.
51. Morina, S.; Kibis, O.; Pervishko, A.; Shelykh, I. Transport properties of a two-dimensional electron gas dressed by light. *Physical Review B* **2015**, *91*, 155312.
52. Kibis, O.; Dini, K.; Iorsh, I.; Shelykh, I. All-optical band engineering of gapped Dirac materials. *Physical Review B* **2017**, *95*, 125401.
53. Iurov, A.; Zhemchuzhna, L.; Gumbs, G.; Huang, D.; Tse, W.K.; Blaise, K.; Ejiogu, C. Floquet engineering of tilted and gapped Dirac bandstructure in 1T′-MoS 2. *Scientific Reports* **2022**, *12*, 21348.

 doi:10.20944/preprints202508.1046.v1

54. Kibis, O. Metal-insulator transition in graphene induced by circularly polarized photons. *Physical Review B* **2010**, *81*, 165433.
55. Iurov, A.; Mattis, M.; Zhemchuzhna, L.; Gumbs, G.; Huang, D. Floquet Modification of the Bandgaps and Energy Spectrum in Flat-Band Pseudospin-1 Dirac Materials. *Applied Sciences* **2024**, *14*, 6027.
56. Kristinsson, K.; Kibis, O.V.; Morina, S.; Shelykh, I.A. Control of electronic transport in graphene by electromagnetic dressing. *Scientific reports* **2016**, *6*, 1–7.
57. Iurov, A.; Gumbs, G.; Huang, D. Exchange and correlation energies in silicene illuminated by circularly polarized light. *Journal of Modern Optics* **2017**, *64*, 913–920.
58. Ho, J.; Lai, Y.; Chiu, Y.H.; Lin, M.F. Landau levels in graphene. *Physica E: Low-dimensional Systems and Nanostructures* **2008**, *40*, 1722–1725.
59. Guinea, F.; Castro Neto, A.; Peres, N. Electronic states and Landau levels in graphene stacks. *Physical Review B—Condensed Matter and Materials Physics* **2006**, *73*, 245426.
60. Gumbs, G.; Iurov, A.; Huang, D.; Zhemchuzhna, L. Revealing Hofstadter spectrum for graphene in a periodic potential. *Physical Review B* **2014**, *89*, 241407.
61. Ezawa, M. Quantum Hall effects in silicene. *Journal of the Physical Society of Japan* **2012**, *81*, 064705.
62. Tabert, C.J.; Nicol, E.J. Magneto-optical conductivity of silicene and other buckled honeycomb lattices. *Physical Review B—Condensed Matter and Materials Physics* **2013**, *88*, 085434.
63. Kuc, A.; Heine, T. The electronic structure calculations of two-dimensional transition-metal dichalcogenides in the presence of external electric and magnetic fields. *Chemical Society Reviews* **2015**, *44*, 2603–2614.
64. He, W.Y.; Zhou, B.T.; He, J.J.; Yuan, N.F.; Zhang, T.; Law, K.T. Magnetic field driven nodal topological superconductivity in monolayer transition metal dichalcogenides. *Communications Physics* **2018**, *1*, 40.
65. Malcolm, J.D.; Nicol, E.J. Magneto-optics of massless Kane fermions: Role of the flat band and unusual Berry phase. *Physical Review B* **2015**, *92*, 035118.
66. Tabert, C.; Carbotte, J.; Nicol, E. Optical and transport properties in three-dimensional Dirac and Weyl semimetals. *Physical Review B* **2016**, *93*, 085426.
67. Rappoport, T.G.; Uchoa, B.; Castro Neto, A. Magnetism and magnetotransport in disordered graphene. *Physical Review B—Condensed Matter and Materials Physics* **2009**, *80*, 245408.
68. Shakouri, K.; Vasilopoulos, P.; Vargiamidis, V.; Peeters, F. Spin-and valley-dependent magnetotransport in periodically modulated silicene. *Physical Review B* **2014**, *90*, 125444.
69. Islam, S.F. Magnetotransport properties of 8-Pmmn borophene: effects of Hall field and strain. *Journal of Physics: Condensed Matter* **2018**, *30*, 275301.
70. Islam, S.F.; Dutta, P. Valley-polarized magnetoconductivity and particle-hole symmetry breaking in a periodically modulated α-T 3 lattice. *Physical Review B* **2017**, *96*, 045418.
71. Nguyen, H.T.; Dinh, L.; Vu, T.V.; Hoa, L.T.; Hieu, N.N.; Nguyen, C.V.; Nguyen, H.V.; Kubakaddi, S.; Phuc, H.V. Quantum magnetotransport properties of silicene: Influence of the acoustic phonon correction. *Physical Review B* **2021**, *104*, 075445.
72. Tymchenko, M.; Nikitin, A.Y.; Martin-Moreno, L. Faraday rotation due to excitation of magnetoplasmons in graphene microribbons. *ACS nano* **2013**, *7*, 9780–9787.
73. Do, T.N.; Gumbs, G.; Shih, P.H.; Huang, D.; Chiu, C.W.; Chen, C.Y.; Lin, M.F. Peculiar optical properties of bilayer silicene under the influence of external electric and magnetic fields. *Scientific reports* **2019**, *9*, 624.
74. Tahir, M.; Vasilopoulos, P. Electrically tunable magnetoplasmons in a monolayer of silicene or germanene. *Journal of Physics: Condensed Matter* **2015**, *27*, 075303.
75. Balassis, A.; Dahal, D.; Gumbs, G.; Iurov, A.; Huang, D.; Roslyak, O. Magnetoplasmons for the α-T3 model with filled Landau levels. *Journal of Physics: Condensed Matter* **2020**, *32*, 485301.
76. Illes, E.; Carbotte, J.; Nicol, E. Hall quantization and optical conductivity evolution with variable Berry phase in the α-T 3 model. *Physical Review B* **2015**, *92*, 245410.
77. Luican, A.; Li, G.; Andrei, E.Y. Quantized Landau level spectrum and its density dependence in graphene. *Physical Review B—Condensed Matter and Materials Physics* **2011**, *83*, 041405.
78. Weekes, N.; Iurov, A.; Zhemchuzhna, L.; Gumbs, G.; Huang, D. Generalized WKB theory for electron tunneling in gapped α- T 3 lattices. *Physical Review B* **2021**, *103*, 165429.